The metabolically protective energy expenditure increase of *Pik3r1*-related insulin resistance is not explained by Ucp1-mediated thermogenesis

Ineke Luijten[1], Ami Onishi[1], Eleanor J. McKay[1], Tore Bengtsson[2], Robert K. Semple[1,3]

[1] Centre for Cardiovascular Science, University of Edinburgh, Edinburgh, UK

[2] Department of Molecular Biosciences, The Wenner-Gren Institute, Stockholm University, Stockholm, Sweden

[3] MRC Human Genetics Unit, Institute of Genetics and Cancer, University of Edinburgh, Edinburgh, UK

Correspondence to:

Prof. Robert K. Semple, Centre for Cardiovascular Science, University of Edinburgh, Queen's Medical Research Institute, Little France Crescent, Edinburgh EH16 4TJ, UK. Tel: +44 131 242 6051/ Email: rsemple@ed.ac.uk

Abstract

Objective: The human *PIK3R1* Y657* mutation impairs phosphoinositide 3-kiase (PI3K) activation, producing insulin resistance (IR) and reduced adiposity but, surprisingly, no fatty liver or dyslipidaemia. Mice heterozygous for *Pik3r1* Y657* metabolically phenocopy humans, moreover exhibiting increased energy expenditure. We suggest that this protects from lipotoxicity despite IR, and here investigate its cause.

Methods: *Pik3r1*$^{Y657*/WT}$ (Pik3r1^{Y657*}) mice and wild-type (WT) littermates single-caged at 21 or 30°C were fed a 45% high-fat diet for 3 weeks. Body composition, food intake, metabolic efficiency, energy expenditure and physical activity were determined. Body temperature and tail heat loss were assessed by infrared imaging, thermal insulation by a modified Scholander experiment, and total Uncoupling Protein 1 (Ucp1)-dependent thermogenic capacity by determining peak norepinephrine-induced oxygen consumption.

Results: Pik3r1^{Y657*} mice at 21°C showed higher energy expenditure than WT mice that was not fully explained by concomitant increase in food intake, nor by changes in physical activity, all as previously reported. No changes were seen in body temperature, tail vein heat dissipation, nor thermal insulation. Moreover, Ucp1-dependent thermogenesis was unaltered. Housing at 30°C did not alter the metabolic phenotype of male Pik3r1^{Y657*} mice, but lowered physical activity and energy expenditure in females. Ucp1-dependent thermogenic capacity at 30°C was unchanged in Pik3r1^{Y657*} mice compared to WT.

Conclusions: The ‘energy leak’ that we suggest is metabolically protective in Pik3r1-related IR in mice and humans is not caused by Ucp1-mediated BAT hyperactivation, nor by impaired thermal insulation. Further metabolic studies are now required to seek alternative explanations such as non Ucp1-mediated futile cycling within or among metabolically important tissues.

Keywords

Insulin resistance, PI 3-Kinase, Pik3r1, energy expenditure, brown adipose tissue, SHORT syndrome

1. Introduction

Insulin resistance (IR) in the general population is closely associated with dyslipidaemia, characterised by high serum triglyceride, low HDL cholesterol, and fatty liver disease (e.g. [1,2]). This is also true in most forms of severe IR of known aetiology, whether genetic or acquired [3,4]. We and others have reported, however, that monogenic forms of severe IR due to loss of function of the insulin receptor or downstream phosphoinositide 3-kinase (PI3K), are an exception to this. Specifically, in both recessive and dominant severe IR caused by *INSR* mutations [5], and in SHORT syndrome, which features severe IR and is caused by heterozygous *PIK3R1* mutations, serum triglyceride concentrations and liver triglyceride contents are surprisingly normal or low [6]. This is particularly noteworthy as humans with SHORT syndrome also often have reduced adipose tissue, and indeed have been labelled lipodystrophic [7–9]. However, true lipodystrophy usually features exaggerated dyslipidaemia and fatty liver [10]. These findings demonstrate that IR is uncoupled from dyslipidaemia in humans when caused by primary proximal insulin signalling defects. What explains this beneficial IR subphenotype is unknown, and elucidating the mechanism holds the promise of suggesting new strategies to mitigate some major IR-related comorbidities.

We have developed and described a mouse model of SHORT syndrome caused by the *Pikr3r1* Y657* mutation [11]. This mutation leads to truncation of all three protein products of the *Pik3r1* gene - p85α/p50α/p55α - in the C-terminal SH2 domain, preventing recruitment of PI3K to phosphorylated tyrosine residues on insulin receptor substrate proteins [7,12–14]. In keeping with this, mice heterozygous for the *Pik3r1* Y657* mutation (Pik3r1^{Y657*} mice) show attenuated intracellular insulin signalling, and thus severe IR [6,11,15]. Pik3r1^{Y657*} mice also show reduced adiposity and resist diet-induced obesity, similar to humans [11]. Also like humans with SHORT syndrome, Pik3r1^{Y657*} mice show no increased liver fat and are hypolipidaemic compared to wild-type (WT) controls in both fed and fasted states. They thus phenocopy the human IR phenotype caused by PI3K hypofunction, and serve as a valid model in which to interrogate the mechanism explaining the apparent protection from dyslipidaemia despite IR.

Studies to date have demonstrated increased energy expenditure in Pik3r1^{Y657*} mice [11], and indeed in several other models of pharmacologically or genetically impaired PI3K signalling [16–23]. This increased energy expenditure could plausibly explain normolipidemia despite IR in SHORT

syndrome, as evidenced by the lipid-lowering effect of brown adipose tissue (BAT) activation in hyperlipidaemic mice [24]. Indeed increased thermogenesis in BAT, and perhaps white adipose tissue[25], is a prime hypothesis to explain the energy expenditure increase seen on PI3K inhibition. This has been suggested by several prior studies of pharmacological or genetic PI3K inhibition, but the evidence presented to date has not been definitive, no mechanism whereby impaired PI3K signalling may activate BAT thermogenesis has been proven [16–18,21,22,26], and no model of a human disease has been studied. Observed BAT activation may in fact be secondary to changes in insulation or heat loss in Pik3r1^{Y657*} mice, as is shown in mouse models of other pathologies [27,28]. This is particularly relevant as all studies in mouse models of impaired PI3K signalling have been performed below murine thermoneutrality (i.e. at 21°C), when BAT thermogenic output is mainly determined by sympathetic drive and the degree to which the animals feel cold [29].

We now set out to investigate the source of the unexplained "energy leak" of the *Pik3r1* Y657* mouse model of SHORT syndrome, assessing BAT activity, heat loss through the tail vein, and thermal insulation.

2. Materials and methods

2.1 Animal model and maintenance

Generation of mice carrying the *Pik3r1* Y657* mutation and an intronic neomycin resistance cassette flanked by loxP sites was previously described [11]. For this study the selection cassette was excised by crossing these mice with CAG-cre expressing mice. Mice heterozygous for the *Pik3r1* Y657* mutation (hereafter Pik3r1^{Y657*} mice) and WT littermate controls were derived by breeding Pik3r1$^{WT/WT}$ and Pik3r1$^{WT/Y657*}$ mice on a C57Bl6/J background. All genotyping was performed by Transnetyx, and no experimental animals expressed cre. Animals were group-housed in individually ventilated cages either at the Biological Research Facility at the University of Edinburgh or at the Experimental Core Facility at Stockholm University, both of which maintained a 12 h/12 h light/dark cycle and a controlled standard humidity (50%). All experiments were carried out under the UK Home Office Animals (Scientific Procedures) Act 1986, following University of Edinburgh ethical review, or under approval by the North Stockholm Animal Ethics Committee.

Until 10 weeks of age, all mice had free access to water and chow diet (CRM, Special Diets Services at University of Edinburgh; Altromin 1324P, Brogaarden at Stockholm University), and were housed at 21°C. At 10 weeks of age, mice were single-caged and either kept at 21°C or moved to 30°C. Experimental procedures began after a 2-week acclimatisation period, at the start of which all animals were put on a 45% high-fat diet (HFD, D12451, Research Diets) provided *ad libitum* throughout the study. Animals were kept on HFD for a maximum of 3 weeks during which the experimental procedures outlined below were performed in various cohorts.

At the end of the experimental period, animals were culled by exposure to increasing concentrations of CO_2, except after the norepinephrine test (see 2.6), when animals were already sedated by pentobarbital injection. When unconscious, nose-anus length was measured using a digital calliper, after which death was confirmed by cervical dislocation. Both lobes of interscapular brown adipose tissue (BAT) and inguinal white adipose tissue (ingWAT) were collected immediately post-mortem, weighed, snap-frozen in liquid nitrogen, and stored at -80°C. For determination of tibia length, the left leg was put in 30% KOH for 45 min, after which the tibia was isolated and its length measured with a digital calliper.

2.2 Determination of metabolic efficiency

Body weight and food weight were measured weekly from 11 weeks of age. Food intake in kJ/day was calculated by dividing weekly food intake in grams by 7 and multiplying by the energy density of the diets (Chow CRM 10.74 kJ/g; Chow Altromin 13.5 kJ/g; HFD 19.8 kJ/g). Body composition was measured by tdNMR using the Bruker Minispec Live Mice Analyzer LF50 (University of Edinburgh), or by MRI using the EchoMRI-100™ (Echo Medical Systems, USA. Stockholm University) at the start (12 weeks old) and end (14 weeks old) of the HFD-feeding period. The change in body composition during these two weeks was calculated as (fat mass end– fat mass start) + (lean mass end– lean mass start) and converted from gram to kJ using 39 kJ/g and 5 kJ/g as energy densities for fat and lean mass respectively. Metabolic efficiency was calculated by dividing the difference in body composition (in kJ) by the food intake (in kJ) over the same period, multiplied by 100.

2.3 Characterisation of energy metabolism

After 2 weeks of HFD feeding (age 14 weeks), animals were placed in temperature-controlled metabolic chambers (Promethion Core system, Sable Systems) for 1 week. In the Promethion system, mice were housed at the same temperature that they had been housed at throughout the study (either 21°C or 30°C), with a 12 h/12 h light/dark cycle and free access to HFD and water. O_2 consumption, CO_2 production, food intake, water intake, and physical activity (XYZ beam breaks) measurements were collected in three-minute intervals. Data collected during the first 3 days was excluded from analyses, as this was considered an acclimatisation period. Data from days 4-6 was extracted and analyzed. Energy expenditure in watts was calculated using a modified Weir equation:

$$EE\ (W) = (0.2716\ \frac{W \times min}{ml} \times vO_2\ consumed\ [\frac{ml}{min}] + 0.07616\ \frac{W \times min}{ml} \times vCO_2\ produced\ [\frac{ml}{min}])$$

and expressed per g lean body mass [28,30].

Food intake was set to 0 at 7AM on day 4 and calculated cumulatively thereafter, before conversion from g to kJ using the energy density of the HFD (see 2.2). Physical activity was calculated as the sum of X-, Y- and Z-bream breaks per time point. The theoretical thermic effect of food was calculated using the thermic effects of fat (2.5%), carbohydrates (7.5%) and protein (25%) [31].

2.4 Assessment of body temperature and heat loss

After 1 week of HFD-feeding (age 13 weeks), tail and inner ear temperatures were measured in mice housed at 21°C using a FLIR® T650sc infrared camera (FLIR Instruments, Germany). To prevent warming of the tail by touching, animals were moved in a cardboard tunnel and placed on top of their cage lid, where they could move freely. At least 4 images were taken per animal from the inner ear and 4 from the tail. Inner ear, tail base and tail temperatures were determined for each image using FLIR Tools Software, and averaged to obtain final values per mouse.

2.5 Assessment of thermal insulation

To compare thermal insulation of WT and Pik3r1^{Y657*} mice housed at 21°C, a modified Scholander experiment [32] was performed. After 2 weeks of HFD-feeding, animals (age 14 weeks) were placed in the Promethion system at 21°C with free access to HFD and water. After a 2.5 day acclimatisation period, the system temperature was first increased to 33°C, maintained for 2h, and then decreased sequentially to 30°C, 25°C, 20°C and 15°C, with every temperature maintained for 2h. O_2

consumption, CO_2 production and physical activity measurements were collected and analyzed. O_2 consumption values at each temperature were averaged from 5 successive points when physical activity, measured by XYZ-beam breaks, was closest to zero. Energy expenditure per gram of lean mass was calculated as described in 2.3.

2.6 Determination of Ucp1-dependent thermogenic capacity

To determine total Ucp1-dependent thermogenic capacity in animals housed at either 21°C or 30°C throughout the study, a norepinephrine (NE) test was performed. First, animals were sedated by intraperitoneal (i.p.) injection of 90 mg/kg pentobarbital (APL, Sweden). Animals were then placed in individual glass cylinders (to lessen air volume, allowing for more sensitive measurements) in the Promethion system at 30°C (to sustain body temperature) and baseline O_2 consumption was measured in three-minute intervals for 20 minutes. Subsequently, animals were briefly taken out of the cylinders and injected i.p. with 1 mg/kg norepinephrine bitartrate salt monohydrate (Sigma, Germany). Animals were put back into the cylinders and O_2 consumption was measured for another 40 minutes. Data was extracted and analyzed, with O_2 consumption expressed per gram lean mass. Total Ucp1-dependent thermogenic capacity was calculated by subtracting baseline O_2 consumption (average of 3 successive stable points) from peak NE-induced O_2 consumption (average of 3 successive highest points).

2.7 Western blot analyses

Total Ucp1 protein in BAT and ingWAT lobes was determined as follows: one lobe of dissected adipose tissue was homogenized with a Teflon pestle in RIPA buffer containing protease (cOmplete™ Mini, Roche, Germany) and phosphatase (5 mM Na fluoride, 1 mM Na orthovanadate) inhibitors. Homogenized samples were kept on ice for 15 min and then centrifuged at 14000x*g* for 15 min at 4°C, after which the protein fraction was transferred to a new tube. Protein concentrations of homogenates were measured using the Lowry method [33] , and total protein (ug) per adipose lobe was calculated (homogenate protein concentration (ug/ul) * RIPA buffer used for lobe homogenization (ul)). 5 ug (BAT) or 10 ug (ingWAT) of protein was separated on a 12% polyacrylamide gel (Mini-PROTEAN® TGX™, BioRad). Proteins were then transferred to a PVDF membrane (BioRad) using a Transblot Turbo system (BioRad) according to manufacturers' instructions. Subsequently,

membranes were blocked in 5% milk (w/v; Semper) in TBS-T for 1h. Membranes were incubated overnight at 4°C in primary anti-Ucp1 antibody (1:15000 solution in 5% milk in TBS-T, antibody kindly gifted by Jan Nedergaard and Barbara Cannon) and anti-αTubulin to control for equal loading (1:1000 solution in 5% milk in TBS-T, Abcam 2144). The following day, membranes were washed and incubated for 1 h with a secondary anti-rabbit antibody (Cell Signaling 7074, 1:10000 in 5 % milk in TBS-T for Ucp1 measurements, 1:1000 for αTubulin measurements). After washing, proteins were visualized using Clarity™ Western ECL Substrate (BioRad) and imaged with a ChemiDoc™ XRS+ Molecular Imager (BioRad). The obtained images were analyzed with Image Lab™ software (BioRad). AU values for Ucp1 bands were normalized to αTubulin band intensity and calculated per ug protein loaded. Total Ucp1/depot (in AU) was calculated by multiplying the amount of Ucp1/ug protein (AU) by the calculated total protein amount (ug) per lobe.

2.8 Statistical analysis

All statistical analyses were done in Graphpad Prism, version 10.1.1. All data are represented as mean ± SEM. For comparison of differences between two groups at a single time-point, a Student's t-test was used. Differences in one parameter between two groups over time were examined by two-way ANOVA followed by Šídák's multiple comparisons test. For comparison of energy expenditure, cumulative food intake, and beam break data obtained by the Promethion system, the area under the curve (AUC) was determined per animal, averages and standard errors were calculated per genotype, and these were then compared by Student's t test. For comparison of slopes and Y-intercepts of energy expenditure in relation to ambient temperature between genotypes, linear regression was performed on data points ranging from 15°C to 30°C.

3. Results

3.1 Pik3r1^{Y657*} mice have decreased metabolic efficiency

We previously reported that heterozygous *Pik3r1* Y657* mice (hereafter simply "Pik3r1^{Y657*} mice") exhibit increased energy expenditure that is not explained by increased locomotor activity [11]. We first set out to reproduce this observation, now studying mice in which the intronic antibiotic resistance cassette has been excised, conducting studies in two different animal facilities.

Individually housed 12-week old WT and Pik3r1^{Y657*} mice were challenged calorically with a 45% HFD, an approach commonly used to impose a load on adipose tissue and unmask lipodystrophic phenotypes [11]. As we previously reported [11], both male and female Pik3r1^{Y657*} mice were smaller than WT littermates (Fig. 1A), with lower body weight (Fig. 1B), body length (Fig. 1C), and tibia length (Fig. 1D). The reduced body weight in Pik3r1^{Y657*} mice was accounted for by reduction of both lean and fat mass, indicating that the mice were proportionally smaller (Figs. 1E, F). Interestingly, fat mass was not significantly different between WT and Pik3r1^{Y657*} mice at the beginning of the HFD-feeding period (Fig. 1F t=0). Despite their smaller size, Pik3r1^{Y657*} mice tended to eat more than WT mice (Fig. 1G t=0). During the first two weeks of HFD feeding, both male and female WT mice became hyperphagic, an effect that decreased by 3 weeks in males and plateaued in females (Fig. 1G). In contrast, Pik3r1^{Y657*} mice showed a smaller increase in food intake from their elevated baseline, and this increase was sustained for both males and females.

Based on changes in lean and fat mass and the total food intake over the first two weeks of HFD feeding, we next calculated metabolic efficiency. Both male and female Pik3r1^{Y657*} mice had lower metabolic efficiency compared to WT littermates (Fig. 1H). This indicates that less of the energy consumed was stored in Pik3r1^{Y657*} mice fed HFD. As we have previously found no evidence for nutritional malabsorption in mice of this genotype [11], this suggests increased energy expenditure as the likely explanation for reduced fat tissue accretion compared to WT littermates.

3.2 Increased energy expenditure in Pik3r1^{Y657*} mice is not explained by increased food intake or physical activity

To determine whether the decreased metabolic efficiency of Pik3r1^{Y657*} mice was indeed associated with greater energy expenditure compared to WT mice, we next undertook indirect calorimetry during the third week of HFD-feeding. To account for the difference in body size between WT and Pik3r1^{Y657*} mice, energy expenditure was normalised to lean body mass, and in both male and female Pik3r1^{Y657*} mice increased lean mass-normalised energy expenditure was confirmed (Figs. 2A, D).

We next investigated the origin of the increased energy expenditure. We first assessed whether there were any changes in the obligatory components of energy expenditure, which consist out of standard metabolic rate, thermic effect of food (i.e. obligatory diet-induced thermogenesis) and physical activity associated with e.g. feeding [34]. To exclude the possibility that the mildly elevated

food intake of the male Pik3r1^{Y657*} mice (Figs. 1G, 2B) was sufficient to account for their increased energy expenditure, we first calculated the extra energy lost due to the obligatory thermic effect of food in Pik3r1^{Y657*} mice. From Fig. 2B, we calculated that male Pik3r1^{Y657*} mice ate on average 18 kJ more energy than WT mice during the light phase. The obligatory thermic effect of the HFD formulation used in this study is 8.75% (based on thermic effects of fat, carbohydrates and protein of 2.5%, 7.5% and 25% respectively [31]), which means that 1.6 kJ additional energy expenditure was attributable to extra food intake for male Pik3r1^{Y657*} mice. However, the same mice expended about 4.3 kJ more energy than WT mice in the light phase (Fig. 2A), thus leaving 2.7 kJ of increased energy expenditure per 12 h unaccounted for. Even more strikingly, female Pik3r1^{Y657*} mice, although showing no increased food intake on HFD (Fig. 2E), still showed increased energy expenditure (Fig. 2D). These findings indicate that increased energy expenditure in Pik3r1^{Y657*} mice of either sex is not fully explained by concomitantly increased food intake.

We next determined whether genotype-related changes in physical activity accounted for the unexplained increase in energy expenditure. Due to the nature of the measurement (XYZ-beam breaks), we measured both obligatory (feeding), and facultative (e.g. exercise and fidgeting) physical activity simultaneously. We found no changes in physical activity between male or female Pik3r1^{Y657*} mice and WT littermates (Figs. 2C, F), excluding another potential cause for the increased energy expenditure.

3.3 No change in thermoregulation and BAT activity in Pik3r1^{Y657*} mice

The other components of energy expenditure that we compared between WT and Pik3r1^{Y657*} mice included cold-induced thermogenesis, which is mediated by skeletal muscle (shivering thermogenesis) and/or BAT (non-shivering thermogenesis), and facultative diet-induced thermogenesis, also predominantly mediated by BAT [34]. Because all mice were housed at a temperature well below their thermoneutral zone (i.e. standard ambient animal house temperature of 21°C [29]) throughout the study, it was plausible that any difference in cold perception between WT and Pik3r1^{Y657*} mice could have translated into a difference in thermoregulatory response, and thus increased energy expenditure, in order to defend body temperature.

To characterize thermoregulation of Pik3r1^{Y657*} mice, we first measured body temperature from the inner ear of the mice using an infrared camera. We found no difference between genotypes

in the males, but a small decrease in female Pik3r1^{Y657*} mice compared to WT (Fig. 3A). We next determined whether the mice showed any differences in heat dissipation through the tail vein, an important mechanism whereby mice defend their body temperature at high (via vasodilation) or low (via vasoconstriction) temperatures, which could plausibly be affected by altered PI3K signaling [35–37]. Again using an infrared camera, we measured tail temperatures at both base and the middle section (Fig. 3B), but found no differences between genotypes in either males or females (Figs. 3C-D), indicating no detectable difference in tail vasoregulation and heat loss.

Thermal insulation is also a determinant of cold sensitivity and thus the amount of energy used to defend body temperature. For mice, insulation is mainly determined by fur and skin thickness [37,38], both factors influenced by the PI3K/Akt signaling pathway (e.g. [39–41]). To determine whether insulation was decreased in Pik3r1^{Y657*} mice, which would likely cause a compensatory increase in heat production to defend body temperature, we performed a modified Scholander experiment in which the effect of graded changes in ambient temperature on energy expenditure is assessed [32]. We found that for both WT and Pik3r1^{Y657*} mice, 30°C was the lower critical temperature for the thermoneutral zone (Fig. 3E). We did not further increase the temperature to determine the upper critical temperature of the thermoneutral zone. When ambient temperature dropped below 30°C, both genotypes of both sexes increased energy expenditure to defend their body temperature, as expected. Although the Pik3r1^{Y657*} mice had higher general energy expenditure compared to WT mice at every ambient temperature ranging from 15-33°C (Fig. 3E, Y-intercepts), the incremental increases in energy expenditure per degree reduction in ambient temperature (Fig. 3E, slopes) were identical between genotypes, thus indicating no difference in insulation between genotypes or sexes.

Finally, we determined total Ucp1-dependent non-shivering thermogenic capacity. Although the similarities in thermoregulatory phenotype between Pik3r1^{Y657*} and WT mice reported here (Figs. 3A-E) render BAT hyperactivation unlikely as a response to increased heat loss, reduced PI3K activity has been suggested to affect BAT *Ucp1* expression directly, and thus could increase BAT activity in a cell- or tissue-autonomous manner [16–18,21]. To determine total Ucp1-dependent thermogenic capacity in Pik3r1^{Y657*} and WT mice, we uncoupled all Ucp1 present in pentobarbital-sedated mice by NE injection and recorded the resulting increase in O_2 consumption (Fig. 3F). Mice of both sexes and genotypes increased O_2 consumption after NE injection, but we found no difference in Ucp1-

dependent thermogenic capacity (i.e. peak NE-induced O_2 consumption – basal O_2 consumption (Fig. 3G). To confirm this finding, we dissected interscapular BAT and inguinal WAT and determined Ucp1 protein levels. No differences were found between genotypes in BAT and ingWAT tissue weight or total protein content (Figs. 3H, 3J&K left panels, 3L), and indeed no differences were found in BAT Ucp1 protein levels, either when expressed per ug protein or calculated per total depot (Figs. 3J, K). No detectable levels of Ucp1 were found in ingWAT, thus also confirming no changes in WAT browning (Fig. 3M).

3.4 Increased energy expenditure persists in male, but not female, Pik3r1^{Y657*} mice at thermoneutrality

In the studies above (Figs. 1-3), we have shown that, despite increased energy expenditure, there is no evidence that Pik3r1^{Y657*} mice have altered thermoregulation or BAT activation. However, one factor complicating interpretation of these studies is that they were performed in mice housed at 21°C throughout their lives, which is below the murine thermoneutral zone. As seen in Fig. 3E, living at 21°C requires mice to double their energy expenditure to defend their body temperature. This makes it difficult to extrapolate results from murine studies to humans, since humans manipulate their environment (clothing, central heating etc.) to live the vast majority of their lives within their thermoneutral zone, thus not needing to increase energy expenditure to defend body temperature. To enhance the potential for extrapolation of our results to human SHORT syndrome, we thus next studied the mice in a 'thermally humanized' environment, i.e. without thermal stress. From 10 weeks of age, WT and Pik3r1^{Y657*} mice were housed at thermoneutrality (30°C), and after a 2-week acclimatisation period, received a HFD caloric challenge for 3 weeks.

Being housed at thermoneutrality did not alter the gross phenotype of the mice, as both male and female Pik3r1^{Y657*} mice had reduced body weight and length compared to their WT counterparts (Figs. 4A, B). Tibia length was also reduced in male Pik3r1^{Y657*} mice, but not in females (Fig. 4C). As for mice housed at 21°C, male and female Pik3r1^{Y657*} mice housed at 30 °C had much reduced lean mass compared to WT mice throughout the study (Fig. 4D), with the pattern of fat mass accumulation upon HFD-feeding also comparable between temperatures (Figs. 1F versus 4E). Thermoneutral housing ablated the difference in food intake between male WT and Pik3r1^{Y657*} mice seen at 21°C (Fig. 4F), but the reduction in metabolic efficiency was maintained (Fig. 4G), as well as the increased

lean mass-normalised energy expenditure (Fig. 4J). Once again, increased energy expenditure of male Pik3r1^{Y657*} mice at thermoneutrality could not be explained by increased food intake or physical activity (Figs. 4K, L).

In females, no significant differences in food intake were found between WT and Pik3r1^{Y657*} mice at 30°C (Fig. 4H, K). However, in contract to the males, the reduced metabolic efficiency seen in female Pik3r1^{Y657*} mice 21°C (Fig. 1H) was not evident at 30°C (Fig. 4I), indicating that thermal stress may influence the energy burning phenotype in Pik3r1^{Y657*} females. Indeed, female Pik3r1^{Y657*} mice at 30°C did not have an increased energy expenditure compared to WT mice (Fig. 4J). The lack of increase in energy expenditure in female Pik3r1^{Y657*} mice at 30°C seemed to stem from a decrease in physical activity (Fig. 4L). Thus, when cold exposed, female Pik3r1^{Y657*} mice may increase physical activity –voluntary or involuntary- to generate the heat needed to defend their body temperature.

3.5 No change in Ucp1-dependent thermogenic capacity at thermoneutrality

Although we did not find an increase in BAT thermogenic capacity that could explain the increased energy expenditure in Pik3r1^{Y657*} mice at 21°C, thermal stress might also complicate interpretation of these results. At 21°C, BAT activity is mainly determined by ongoing sympathetic output to the tissue in an effort to defend body temperature, and such continuous activation may mask any direct effects of impaired PI3K signaling on BAT. Thus, we finally determined Ucp1-dependent thermogenic capacity in WT and Pik3r1^{Y657*} mice housed at thermoneutrality.

As shown in Fig. 5A, the increase in O_2 consumption after NE injection was much lower in both male and female WT and Pik3r1^{Y657*} mice housed at 30°C than in mice housed at 21°C (Fig. 3F), reflecting the expected involution of BAT in the absence of thermal stress. However, no difference in NE-induced O_2 consumption was again seen between genotypes (Figs. 5 A,B). This was confirmed by western blot analyses (Figs. 5C-H), thus again indicating no increase in Ucp1-dependent thermogenesis in Pik3r1^{Y657*} mice.

4. Discussion

Fatty liver and metabolic dyslipidaemia are common, major complications of idiopathic, genetic and acquired forms of IR. However, severe IR caused by defects in the insulin receptor or PI3K is not

associated with these complications [6,42]. Studying proximal insulin signalling defects may thus provide novel, important insights into approaches for mitigating IR-associated complications.

We previously showed that Pik3r1^{Y657*} mice phenocopy human SHORT syndrome, featuring severe IR and reduced adiposity, but neither fatty liver nor dyslipidemia [11]. We now confirm the robust increase in lean mass normalized-energy expenditure that we reported previously in male Pik3r1^{Y657*} mice at 21°C in both males and females [11]. This finding has now been reproduced in studies across three different animal facilities, and is consistent with growing evidence that inhibiting PI3K signaling pharmacologically or genetically stimulates energy expenditure in rodents and primates [16–23].

SHORT syndrome has often been described as featuring lipodystrophy. However, although it does usually feature low adiposity and sometimes a regional deficiency of adipose tissue, this alone is insufficient to prove lipodystrophy. Lipodystrophy denotes a failure to accumulate adipose tissue despite a positive energy balance, and is characteristically associated with evidence of ”adipose failure” in the form of adipose hypertrophy and inflammation, dyslipidaemia and ectopic lipid accumulation, particularly in the liver. We have previously failed to demonstrate features of adipose failure in Pik3r1^{Y657*} mice not only when fed a chow diet, but more strikingly also in the fed state while on a 45% HFD [11]. In true lipodystrophy, a HFD caloric challenge would sharply exacerbate metabolic complications. In contrast, we find no metabolic complications in Pik3r1^{Y657*} mice, but we do consistently find increased energy expenditure. Our interpretation is that SHORT syndrome does not feature true lipodystrophy, but that the reduced adipose tissue with healthy lipid phenotype and preserved serum adiponectin concentration is instead a result of increased energy expenditure. This remains to be tested in humans, however.

To determine the mechanism of increased energy expenditure in Pik3r1^{Y657*} mice, we tested different components of energy expenditure and ruled out increased obligatory diet-induced thermogenesis or physical activity as explanations. We also found no indication of increased Ucp1-dependent thermogenesis, neither secondary to other changes in thermoregulation, nor tissue-autonomous. This is surprising, as in several prior studies in an array of rodent models of impaired PI3K signalling, increased BAT thermogenesis was suggested to account for increased energy expenditure [16–18,21,22]. This was not the case in all models, however, as no involvement of BAT [43] and even a downregulation of BAT activity has also been reported [26]. The discrepancy between

the results reported here and the literature may reflect the measurements used. Several studies have reported increased glucose uptake into BAT [17,18] and an upregulation of *Ucp1* gene expression in BAT and ingWAT either *in vivo* [17,18,21], *ex vivo* [18], or *in vitro* [16,18,21]. However, BAT glucose uptake is disconnected from the amount of Ucp1 in, and thus thermogenic capacity of, BAT, as Ucp1 ablation does not decrease BAT glucose uptake [44]. Moreover, the use of *Ucp1* mRNA levels as a proxy for BAT recruitment may provide inadequate results, as Ucp1 only contributes to energy expenditure when uncoupled upon adrenergic stimulation [45]. We have here directly assessed total thermogenic capacity by injecting NE into anaesthetized WT and Pik3r1^{Y657*} mice and quantifying the increase in O_2 consumption. Similar measurements have been reported in one other study [17], but increased basal O_2 consumption due to impaired PI3K signalling was unaccounted for in analysis. We here expressed Ucp1-dependent thermogenic capacity as peak NE-induced O_2 consumption - baseline O_2 consumption, and found no difference between genotypes.

Measurements of Ucp1 protein in BAT or ingWAT are offered as evidence for increased thermogenic activity in some models of attenuated PI3K signaling [16,17,22]. However, the approach taken to quantification is important and can mislead. We here measured Ucp1 protein levels in BAT and ingWAT to confirm the results of the NE-test, but calculated Ucp1 protein levels quantitively per whole BAT depot, instead of only per ug protein. This accounts for any changes in total protein content, and thus dilution of Ucp1 protein, as reported in other models [28,46,47]. Quantitative determination of total Ucp1 protein levels corroborated results of NE testing, showing no changes in BAT activity in Pik3r1^{Y657*} mice compared to WT littermates.

Nearly all studies investigating mice with impaired PI3K signaling have been performed in mice housed at 21°C, i.e. below murine thermoneutrality [29]. We show that without thermal stress, energy expenditure remains increased in male Pik3r1^{Y657*} mice compared to WT. Interestingly, the energy expenditure difference in female mice at 21°C is ablated by thermoneutral housing, likely due to a decrease in physical activity. It is thus likely that, upon cold exposure, female Pik3r1^{Y657*} mice increase physical activity, either voluntary or involuntary, to defend their body temperature, whereas male mice do not. We further report no difference in whole body Ucp1-dependent thermogenic capacity between male and female Pik3r1^{Y657*} mice at 30°C. This suggests that, contrary to previous suggestions [17,18], impaired PI3K signalling in itself does not increase sympathetic output to thermogenic adipose tissue, nor increases *Ucp1* expression in a cell autonomous manner.

We provide strong evidence that the increased energy expenditure in a SHORT syndrome model is not caused by Ucp1-medaited BAT hyperactivity, altered thermoregulation, increased diet-induced thermogenesis or increased physical activity. Previous study of Pik3r1^{Y657*} mice also ruled out increased energy loss via nutritional malabsorption [11]. This leaves the question of the mechanism underlying increased energy expenditure in Pik3r1^{Y657*} mice unresolved. One explanation put forward for increased energy expenditure induced by impaired PI3K signaling is an overall increase in oxidative phosphorylation, translating into an increased basal metabolic rate (BMR) [17,18,20]. In mice and MEFS overexpressing PTEN, increased mitochondrial oxidative phosphorylation caused by increased total mitochondrial network volume has been reported [20], while in mice receiving a clinically utilized PI3K P110α inhibitor, mitochondrial respiration was found to be upregulated [43]. Whether such an increase is the cause or consequence of increased oxidative metabolism is not established, however.

Another non mutually exclusive possibility is increased metabolic futile cycling. Although Ucp1-mediated proton flux is the best studied futile cycle, several others are known, some cell or tissue autonomous (e.g. via the mitochondrial ADP/ATP carrier [48], muscle protein synthesis/degradation [49]), some operating between tissues (e.g. Cori [50] or glyceroneogenesis-lipid cycles [51]), and some that can operate both within a tissue and between tissues (e.g. the glycerolipid-free fatty acid cycle [52]). In this last cycle, triacylglycerols are hydrolysed, with some resulting fatty acids re-esterified into triacylglycerols. There is keen interest in exploiting such cycles to combat obesity and metabolic disease [53]. Metabolic fluxes have not yet been assessed in *Pik3r1*$^{Y657*/WT}$ mice, however static metabolic assessments in fed and fasting states have suggested increased net fatty acid oxidation in the fed state and altered profiles of plasma amino acids.

Finally, our previously reported observation that Pik3r1^{Y657*} mice have larger hearts than WT mice when corrected for body mass [11] may also hold clues. The heart accounts for around 10% of basal metabolic rate in healthy humans [54], variations in its size have been suggested to contribute to alterations in BMR [55,56], and in some circumstances the heart can influence energy expenditure in remote tissues through circulating mediators [57,58]. Whether the enlarged hearts in *Pik3r1*$^{Y657*/WT}$ mice consume more energy themselves, and whether the enlarged heart influences other tissues in this case remains to be determined.

5. Conclusions

Pik3r1^{Y657*} mice, which model the insulin resistance, diet-induced obesity resistance and lack of dyslipidaemia of human SHORT syndrome, have a highly reproducible, unexplained increase in energy expenditure. This is seen both at 21°C and thermoneutrality in males and is not fully explained by increased food intake, locomotor activity, impaired thermal insulation or increased Ucp1-dependent thermogenic capacity. We hypothesise that the increased energy expenditure in Pik3r1^{Y657*} mice might be due to an overall increased mitochondrial respiration, non Ucp-1 mediated metabolic futile cycling, or enlarged hearts. However, studies will be required to test this.

Funding

RKS is supported by the Wellcome Trust [210752] and the BHF Centre for Research Excellence Award III [RE/18/5/34216], and IL by the Swedish Research Council (2019-06422). EJM is supported by a British Heart Foundation (BHF) PhD studentship [FS/18/57/34178].

Author Contributions

IL: conceptualization, methodology, formal analysis, investigation, writing - original draft, writing - review & editing, visualization, funding acquisition. **AO:** methodology, investigation, writing - review & editing. **EM:** investigation, writing - review & editing. **TB:** resources, writing - review & editing. **RKS:** conceptualization, resources, writing - original draft, writing - review & editing, supervision, funding acquisition.

Acknowledgements

We thank Jan Nedergaard and Barbara Cannon for kindly gifting the Ucp1 antibody and for providing feedback on methodology. We thank Roland Stimson for providing access to the FLIR thermal camera, and Nik Morton for access to the TD-NMR machine at the University of Edinburgh. We are grateful for the excellent technical assistance at the Biological Research Facility at the University of Edinburgh and at the Experimental Core Facility at Stockholm University.

Declaration of interest

RS has received consulting fees from Astra Zeneca and Alnylam, and speaking fees from Novo Nordisk, Eli Lilly, and Amryt, all relating to severe insulin resistance and/or lipodystrophy.

References

[1] Gastaldelli, A., Kozakova, M., Højlund, K., Flyvbjerg, A., Favuzzi, A., Mitrakou, A., et al., 2009. Fatty liver is associated with insulin resistance, risk of coronary heart disease, and early atherosclerosis in a large European population. Hepatology (Baltimore, Md.) 49(5): 1537–44, Doi: 10.1002/hep.22845.

[2] Bonora, E., Kiechl, S., Willeit, J., Oberhollenzer, F., Egger, G., Targher, G., et al., 1998. Prevalence of insulin resistance in metabolic disorders: the Bruneck Study. Diabetes 47(10): 1643–9, Doi: 10.2337/diabetes.47.10.1643.

[3] Savage, D.B., Semple, R.K., 2010. Recent insights into fatty liver, metabolic dyslipidaemia and their links to insulin resistance. Current Opinion in Lipidology 21(4): 329–36, Doi: 10.1097/MOL.0b013e32833b7782.

[4] Semple, R.K., Savage, D.B., Cochran, E.K., Gorden, P., O'Rahilly, S., 2011. Genetic syndromes of severe insulin resistance. Endocrine Reviews 32(4): 498–514, Doi: 10.1210/er.2010-0020.

[5] Semple, R.K., Sleigh, A., Murgatroyd, P.R., Adams, C.A., Bluck, L., Jackson, S., et al., 2009. Postreceptor insulin resistance contributes to human dyslipidemia and hepatic steatosis. The Journal of Clinical Investigation 119(2): 315–22, Doi: 10.1172/JCI37432.

[6] Huang-Doran, I., Tomlinson, P., Payne, F., Gast, A., Sleigh, A., Bottomley, W., et al., 2016. Insulin resistance uncoupled from dyslipidemia due to C-terminal PIK3R1 mutations. JCI Insight 1(17), Doi: 10.1172/JCI.INSIGHT.88766.

[7] Chudasama, K.K., Winnay, J., Johansson, S., Claudi, T., König, R., Haldorsen, I., et al., 2013. SHORT syndrome with partial lipodystrophy due to impaired phosphatidylinositol 3 kinase signaling. American Journal of Human Genetics 93(1): 150–7, Doi: 10.1016/j.ajhg.2013.05.023.

[8] Innes, A.M., Dyment, D.A., 1993. SHORT Syndrome.

[9] Avila, M., Dyment, D.A., Sagen, J. V., St-Onge, J., Moog, U., Chung, B.H.Y., et al., 2016. Clinical reappraisal of SHORT syndrome with PIK3R1 mutations: toward recommendation for molecular testing and management. Clinical Genetics 89(4): 501–6, Doi: 10.1111/cge.12688.

[10] Lim, K., Haider, A., Adams, C., Sleigh, A., Savage, D.B., 2021. Lipodistrophy: a paradigm for understanding the consequences of "overloading" adipose tissue. Physiological Reviews 101(3): 907–93, Doi: 10.1152/physrev.00032.2020.

[11] Kwok, A., Zvetkova, I., Virtue, S., Luijten, I., Huang-Doran, I., Tomlinson, P., et al., 2020. Truncation of Pik3r1 causes severe insulin resistance uncoupled from obesity and dyslipidaemia by increased energy expenditure. Molecular Metabolism 40, Doi: 10.1016/j.molmet.2020.101020.

[12] Thauvin-Robinet, C., Auclair, M., Duplomb, L., Caron-Debarle, M., Avila, M., St-Onge, J., et al., 2013. PIK3R1 mutations cause syndromic insulin resistance with lipoatrophy. American Journal of Human Genetics 93(1): 141–9, Doi: 10.1016/j.ajhg.2013.05.019.

[13] Dyment, D.A., Smith, A.C., Alcantara, D., Schwartzentruber, J.A., Basel-Vanagaite, L., Curry, C.J., et al., 2013. Mutations in PIK3R1 cause SHORT syndrome. American Journal of Human Genetics 93(1): 158–66, Doi: 10.1016/j.ajhg.2013.06.005.

[14] Tomlinson, P.R., Knox, R., Perisic, O., Su, H.C., Williams, R.L., Semple, R.K., 2023. Paradoxical dominant negative activity of an immunodeficiency-associated activating PIK3R1 variant 2 3, Doi: 10.1101/2023.11.02.565250.

[15] Winnay, J.N., Solheim, M.H., Dirice, E., Sakaguchi, M., Noh, H.-L., Kang, H.J., et al., 2016. PI3-kinase mutation linked to insulin and growth factor resistance in vivo. The Journal of Clinical Investigation 126(4): 1401–12, Doi: 10.1172/JCI84005.

[16] Ortega-Molina, A., Lopez-Guadamillas, E., Mattison, J.A., Mitchell, S.J., Muñoz-Martin, M., Iglesias, G., et al., 2015. Pharmacological inhibition of PI3K reduces adiposity and metabolic syndrome in obese mice and rhesus monkeys. Cell Metabolism 21(4): 558–70, Doi: 10.1016/j.cmet.2015.02.017.

[17] Araiz, C., Yan, A., Bettedi, L., Samuelson, I., Virtue, S., McGavigan, A.K., et al., 2019. Enhanced β-adrenergic signalling underlies an age-dependent beneficial metabolic effect of PI3K p110α inactivation in adipose tissue. Nature Communications 10(1): 1546, Doi: 10.1038/s41467-019-09514-1.

[18] Ortega-Molina, A., Efeyan, A., Lopez-Guadamillas, E., Muñoz-Martin, M., Gómez-López, G., Cañamero, M., et al., 2012. Pten positively regulates brown adipose function, energy expenditure, and longevity. Cell Metabolism 15(3): 382–94, Doi: 10.1016/j.cmet.2012.02.001.

[19] Lopez-Guadamillas, E., Muñoz-Martin, M., Martinez, S., Pastor, J., Fernandez-Marcos, P.J., Serrano, M., 2016. PI3Kα inhibition reduces obesity in mice. Aging 8(11): 2747–53, Doi: 10.18632/aging.101075.

[20] Garcia-Cao, I., Song, M.S., Hobbs, R.M., Laurent, G., Giorgi, C., de Boer, V.C.J., et al., 2012. Systemic elevation of PTEN induces a tumor-suppressive metabolic state. Cell 149(1): 49–62, Doi: 10.1016/j.cell.2012.02.030.

[21] Song, N.-J., Chang, S.-H., Kim, S., Panic, V., Jang, B.-H., Yun, U.J., et al., 2018. PI3Ka-Akt1-mediated Prdm4 induction in adipose tissue increases energy expenditure, inhibits weight gain, and improves insulin resistance in diet-induced obese mice. Cell Death & Disease 9(9): 876, Doi: 10.1038/s41419-018-0904-3.

[22] Perino, A., Beretta, M., Kilić, A., Ghigo, A., Carnevale, D., Repetto, I.E., et al., 2014. Combined inhibition of PI3Kβ and PI3Kγ reduces fat mass by enhancing α-MSH-dependent sympathetic drive. Science Signaling 7(352): ra110, Doi: 10.1126/scisignal.2005485.

[23] Zhang, Z., Turer, E., Li, X., Zhan, X., Choi, M., Tang, M., et al., 2016. Insulin resistance and diabetes caused by genetic or diet-induced KBTBD2 deficiency in mice. Proceedings of the National Academy of Sciences of the United States of America 113(42): E6418–26, Doi: 10.1073/pnas.1614467113.

[24] Berbée, J.F.P., Boon, M.R., Khedoe, P.P.S.J., Bartelt, A., Schlein, C., Worthmann, A., et al., 2015. Brown fat activation reduces hypercholesterolaemia and protects from atherosclerosis development. Nature Communications 6: 6356, Doi: 10.1038/ncomms7356.

[25] Kalinovich, A. V., de Jong, J.M.A., Cannon, B., Nedergaard, J., 2017. UCP1 in adipose tissues: two steps to full browning. Biochimie 134: 127–37, Doi: 10.1016/j.biochi.2017.01.007.

[26] Nelson, V.L.B., Jiang, Y.-P., Dickman, K.G., Ballou, L.M., Lin, R.Z., 2014. Adipose tissue insulin resistance due to loss of PI3K p110α leads to decreased energy expenditure and obesity. American Journal of Physiology. Endocrinology and Metabolism 306(10): E1205-16, Doi: 10.1152/ajpendo.00625.2013.

[27] Warner, A., Rahman, A., Solsjö, P., Gottschling, K., Davis, B., Vennström, B., et al., 2013. Inappropriate heat dissipation ignites brown fat thermogenesis in mice with a mutant thyroid hormone receptor α1. Proceedings of the National Academy of Sciences of the United States of America 110(40): 16241–6, Doi: 10.1073/pnas.1310300110.
[28] Fischer, A.W., Hoefig, C.S., Abreu-Vieira, G., de Jong, J.M.A., Petrovic, N., Mittag, J., et al., 2016. Leptin Raises Defended Body Temperature without Activating Thermogenesis. Cell Reports 14(7): 1621–31, Doi: 10.1016/j.celrep.2016.01.041.
[29] Cannon, B., Nedergaard, J., 2011. Nonshivering thermogenesis and its adequate measurement in metabolic studies. The Journal of Experimental Biology 214(Pt 2): 242–53, Doi: 10.1242/jeb.050989.
[30] Weir, J.B.D.B., 1949. New methods for calculating metabolic rate with special reference to protein metabolism. The Journal of Physiology 109(1–2): 1–9, Doi: 10.1113/jphysiol.1949.sp004363.
[31] Trumbo, P., Schlicker, S., Yates, A.A., Poos, M., Food and Nutrition Board of the Institute of Medicine, T.N.A., 2002. Dietary reference intakes for energy, carbohydrate, fiber, fat, fatty acids, cholesterol, protein and amino acids. Journal of the American Dietetic Association 102(11): 1621–30, Doi: 10.1016/s0002-8223(02)90346-9.
[32] Scholander, P.F., Hock, R., Walters, V., Johnson, F., Irving, L., 1950. Heat regulation in some arctic and tropical mammals and birds. The Biological Bulletin 99(2): 237–58, Doi: 10.2307/1538741.
[33] Lowry, O.H., Rosebrough, N.J., Farr, A.L., Randall, R.J., 1951. Protein measurement with the Folin phenol reagent. The Journal of Biological Chemistry 193(1): 265–75.
[34] van Marken Lichtenbelt, W.D., Schrauwen, P., 2011. Implications of nonshivering thermogenesis for energy balance regulation in humans. American Journal of Physiology. Regulatory, Integrative and Comparative Physiology 301(2): R285-96, Doi: 10.1152/ajpregu.00652.2010.
[35] Morello, F., Perino, A., Hirsch, E., 2009. Phosphoinositide 3-kinase signalling in the vascular system. Cardiovascular Research 82(2): 261–71, Doi: 10.1093/cvr/cvn325.
[36] Olver, T.D., Grunewald, Z.I., Ghiarone, T., Restaino, R.M., Sales, A.R.K., Park, L.K., et al., 2019. Persistent insulin signaling coupled with restricted PI3K activation causes insulin-induced vasoconstriction. American Journal of Physiology. Heart and Circulatory Physiology 317(5): H1166–72, Doi: 10.1152/ajpheart.00464.2019.
[37] Gordon, C.J., 2017. The mouse thermoregulatory system: Its impact on translating biomedical data to humans. Physiology & Behavior 179: 55–66, Doi: 10.1016/j.physbeh.2017.05.026.
[38] Fischer, A.W., Csikasz, R.I., von Essen, G., Cannon, B., Nedergaard, J., 2016. No insulating effect of obesity. American Journal of Physiology. Endocrinology and Metabolism 311(1): E202-13, Doi: 10.1152/ajpendo.00093.2016.
[39] Teng, Y., Fan, Y., Ma, J., Lu, W., Liu, N., Chen, Y., et al., 2021. The PI3K/Akt Pathway: Emerging Roles in Skin Homeostasis and a Group of Non-Malignant Skin Disorders. Cells 10(5), Doi: 10.3390/cells10051219.
[40] Pérez-Mora, S., Ocampo-López, J., Gómez-García, M.D.C., Pérez-Ishiwara, D.G., 2023. BFNB Enhances Hair Growth in C57BL/6 Mice through the Induction of EGF and FGF7 Factors and the PI3K-AKT-β-Catenin Pathway. International Journal of Molecular Sciences 24(15), Doi: 10.3390/ijms241512110.

[41] Chen, Y., Fan, Z., Wang, X., Mo, M., Zeng, S. Bin., Xu, R.-H., et al., 2020. PI3K/Akt signaling pathway is essential for de novo hair follicle regeneration. Stem Cell Research & Therapy 11(1): 144, Doi: 10.1186/s13287-020-01650-6.
[42] Semple, R.K., Sleigh, A., Murgatroyd, P.R., Adams, C.A., Bluck, L., Jackson, S., et al., 2009. Postreceptor insulin resistance contributes to human dyslipidemia and hepatic steatosis. The Journal of Clinical Investigation 119(2): 315–22, Doi: 10.1172/JCI37432.
[43] Hedges, C.P., Shetty, B., Broome, S.C., MacRae, C., Koutsifeli, P., Buckels, E.J., et al., 2023. Dietary supplementation of clinically utilized PI3K p110α inhibitor extends the lifespan of male and female mice. Nature Aging 3(2): 162–72, Doi: 10.1038/s43587-022-00349-y.
[44] Olsen, J.M., Csikasz, R.I., Dehvari, N., Lu, L., Sandström, A., Öberg, A.I., et al., 2017. β3-Adrenergically induced glucose uptake in brown adipose tissue is independent of UCP1 presence or activity: Mediation through the mTOR pathway. Molecular Metabolism 6(6): 611–9, Doi: 10.1016/j.molmet.2017.02.006.
[45] Nedergaard, J., Cannon, B., 2013. UCP1 mRNA does not produce heat. Biochimica et Biophysica Acta 1831(5): 943–9, Doi: 10.1016/j.bbalip.2013.01.009.
[46] Luijten, I.H.N., Brooks, K., Boulet, N., Shabalina, I.G., Jaiprakash, A., Carlsson, B., et al., 2019. Glucocorticoid-Induced Obesity Develops Independently of UCP1. Cell Reports 27(6): 1686-1698.e5, Doi: 10.1016/j.celrep.2019.04.041.
[47] Luijten, I.H.N., Cannon, B., Nedergaard, J., 2019. Glucocorticoids and Brown Adipose Tissue: Do glucocorticoids really inhibit thermogenesis? Molecular Aspects of Medicine: 42–59, Doi: 10.1016/j.mam.2019.07.002.
[48] Bertholet, A.M., Chouchani, E.T., Kazak, L., Angelin, A., Fedorenko, A., Long, J.Z., et al., 2019. H+ transport is an integral function of the mitochondrial ADP/ATP carrier. Nature 571(7766): 515–20, Doi: 10.1038/s41586-019-1400-3.
[49] Sharma, A., Oonthonpan, L., Sheldon, R.D., Rauckhorst, A.J., Zhu, Z., Tompkins, S.C., et al., 2019. Impaired skeletal muscle mitochondrial pyruvate uptake rewires glucose metabolism to drive whole-body leanness. ELife 8, Doi: 10.7554/eLife.45873.
[50] She, P., Reid, T.M., Bronson, S.K., Vary, T.C., Hajnal, A., Lynch, C.J., et al., 2007. Disruption of BCATm in mice leads to increased energy expenditure associated with the activation of a futile protein turnover cycle. Cell Metabolism 6(3): 181–94, Doi: 10.1016/j.cmet.2007.08.003.
[51] Guan, H.-P., Li, Y., Jensen, M.V., Newgard, C.B., Steppan, C.M., Lazar, M.A., 2002. A futile metabolic cycle activated in adipocytes by antidiabetic agents. Nature Medicine 8(10): 1122–8, Doi: 10.1038/nm780.
[52] Reshef, L., Olswang, Y., Cassuto, H., Blum, B., Croniger, C.M., Kalhan, S.C., et al., 2003. Glyceroneogenesis and the triglyceride/fatty acid cycle. The Journal of Biological Chemistry 278(33): 30413–6, Doi: 10.1074/jbc.R300017200.
[53] Brownstein, A.J., Veliova, M., Acin-Perez, R., Liesa, M., Shirihai, O.S., 2022. ATP-consuming futile cycles as energy dissipating mechanisms to counteract obesity. Reviews in Endocrine & Metabolic Disorders 23(1): 121–31, Doi: 10.1007/s11154-021-09690-w.
[54] Löffler, M.C., Betz, M.J., Blondin, D.P., Augustin, R., Sharma, A.K., Tseng, Y.-H., et al., 2021. Challenges in tackling energy expenditure as obesity therapy: From preclinical models to clinical application. Molecular Metabolism 51: 101237, Doi: 10.1016/j.molmet.2021.101237.
[55] Konarzewski, M., Diamond, J., 1995. Evolution of basal metabolic rate and organ masses in laboratory mice. Evolution; International Journal of Organic Evolution 49(6): 1239–48, Doi: 10.1111/j.1558-5646.1995.tb04450.x.

[56] Selman, C., Lumsden, S., Bünger, L., Hill, W.G., Speakman, J.R., 2001. Resting metabolic rate and morphology in mice (Mus musculus) selected for high and low food intake. The Journal of Experimental Biology 204(Pt 4): 777–84, Doi: 10.1242/jeb.204.4.777.

[57] Collins, S., 2014. A heart-adipose tissue connection in the regulation of energy metabolism. Nature Reviews. Endocrinology 10(3): 157–63, Doi: 10.1038/nrendo.2013.234.

[58] Baskin, K.K., Grueter, C.E., Kusminski, C.M., Holland, W.L., Bookout, A.L., Satapati, S., et al., 2014. MED13-dependent signaling from the heart confers leanness by enhancing metabolism in adipose tissue and liver. EMBO Molecular Medicine 6(12): 1610–21, Doi: 10.15252/emmm.201404218.

Figure legends

Figure 1. Male and female Pik3r1^{Y657*} mice at 21 °C show reduced metabolic efficiency. Male (green) and female (orange) WT and Pik3r1^{Y657*} mice were fed a 45% HFD from t=0 (12 weeks old, indicated by dotted lines) and kept at 21 °C for the duration of the study. Boxes with 'IC' represent periods in the indirect calorimetry system. (A) Representative images at 15 weeks old. (B) Body weight over time. (C) Body length (nose-anus) at 15 weeks old. (D) Tibia length at 15 weeks old. (E) Lean mass over time. (F) Fat mass over time. (G) Food intake expressed per gram lean mass over time. (H) Metabolic efficiency calculated between 12-14 weeks old. All data are represented as mean ± SEM, error bars may be too small to be visible; Male WT N=10, Male Pik3r1^{Y657*} N=8, Female WT N=9, Female Pik3r1^{Y657*} N=6. * P<0.05, ** p<0.01, *** p<0.001 and **** p<0.0001. Two-way ANOVA with Šídák's multiple comparisons test, significance per timepoint between genotypes (B, E-G); Student's t test (C, D, H).

Figure 2. Energy metabolism in Pik3r1^{Y657*} mice at 21 °C. Male (green) and female (orange) WT and Pik3r1^{Y657*} mice were fed a 45% HFD and kept at 21 °C for the duration of the study. Grey boxes represent dark phases. (A, D) 72h energy expenditure calculated as Watt / lean mass. (B, E) Cumulative food intake calculated in kJ. (C, F) Sum of X, Y and Z beam breaks per time point. All data are represented as mean ± SEM (shaded areas); Male WT N=10, Male Pik3r1^{Y657*} N=8, Female WT N=9, Female Pik3r1^{Y657*} N=6. NS = non-significant, **** p<0.0001. AUC determined per animal and averaged per genotype, compared by Student's t test (A-F).

Figure 3. Tail vein heat dissipation, insulation, and Ucp1-dependent thermogenic capacity in Pik3r1^{Y657*} mice at 21 °C. Male (green) and female (orange) WT and Pik3r1^{Y657*} mice were fed a 45% HFD and kept at 21 °C for the duration of the study. (A) Body temperature measured from the inner ear at 14 weeks old. (B) Representative thermal images at 14 weeks old. Black arrows indicate tail areas used for quantification of temperature. (C) Quantification of tail base temperature. (D) Quantification of temperature at the middle of the tail. (E) Energy expenditure calculated as Watt / lean mass in relationship to ambient temperature (Ta). (F) Norepinephrine (NE)-induced oxygen consumption in pentobarbital-anaesthetized mice. (G) Quantification of (F): Ucp1-dependent

thermogenic capacity = peak NE-induced O_2 consumption – basal O_2 consumption. (H) Total BAT weight. (I) Representative immunoblots showing Ucp1 protein in BAT homogenates with αTubulin as a loading control.
(J,K) Quantification of (I) showing Ucp1 per microgram protein, total protein per depot, and total Ucp1 per depot. (L) Total ingWAT weight. (M) Representative immunoblots showing Ucp1 protein in ingWAT homogenates with αTubulin as a loading control. All data are represented as mean ± SEM, error bars may be too small to be visible; Male WT N=8, Male Pik3r1^{Y657*} N=3, Female WT N=7, Female Pik3r1^{Y657*} N=6 (A, C, D). Male WT N=6, Male Pik3r1^{Y657*} N=3, Female WT N=6, Female Pik3r1^{Y657*} N=7 (E). Male WT N=10, Male Pik3r1^{Y657*} N=8, Female WT N=9, Female Pik3r1^{Y657*} N=6 (F-M). NS = non-significant, * P<0.05, ** P<0.01. Student's t test (A, C, D, G-L); Linear regression on data points from 15 °C to 30 °C, slope and Y-intercept comparison between genotypes (E).

Figure 4. Energy metabolism of Pik3r1^{Y657*} mice at 30°C. Male (green) and female (orange) WT and Pik3r1^{Y657*} mice were fed a 45% HFD from t=0 (12 weeks old, indicated by dotted lines) and kept at 30 °C for the duration of the study. Boxes with 'IC' represent periods in the indirect calorimetry system. Grey boxes represent dark phases. (A) Body weight over time. (B) Body length (nose-anus) at 15 weeks old. (C) Tibia length at 15 weeks old. (D) Lean mass over time. (E) Fat mass over time. (F, H) Food intake expressed per gram lean mass over. (G, I) Metabolic efficiency calculated between 12-14 weeks old. (J) 72h energy expenditure calculated as Watt / lean mass. (K) Cumulative food intake calculated in kJ. (L) Sum of X, Y and Z beam breaks per time point. All data are represented as mean ± SEM (shaded areas in J-M), error bars may be too small to be visible; Male WT N=10, Male Pik3r1^{Y657*} N=7, Female WT N=7, Female Pik3r1^{Y657*} N=9. NS = non-significant, * P<0.05, ** p<0.01, *** p<0.001 and **** p<0.0001. Two-way ANOVA with Šídák's multiple comparisons test, significance per timepoint between genotypes (A, D-F, H); Student's t test (B, C, G, I), AUC determined per animal and averaged per genotype, compared by Student's t test (J-L).

Figure 5. No BAT hyperactivation in Pik3r1^{Y657*} mice at 30 °C. Male (green) and female (orange) WT and Pik3r1^{Y657*} mice were fed a 45% HFD and kept at 30 °C for the duration of the study. (A) Norepinephrine (NE, 1mg/kg)-induced oxygen consumption in pentobarbital-anaesthetized mice. (B) Quantification of (A): Ucp1-dependent thermogenic capacity = peak NE-induced O_2 consumption –

basal O_2 consumption. (C) Total BAT weight. (D) Representative immunoblots showing Ucp1 protein in BAT homogenates with αTubulin as a loading control. (E) Quantification of (D) showing Ucp1 per microgram protein, total protein per depot, and total Ucp1 per depot. (F) Total ingWAT weight. (G) Total protein per depot. (H) Representative immunoblots showing Ucp1 protein in ingWAT homogenates with αTubulin as a loading control. All data are represented as mean ± SEM, error bars may be too small to be visible; Male WT N=10, Male Pik3r1^{Y657*} N=7, Female WT N=7, Female Pik3r1^{Y657*} N=9. * $P<0.05$, *** $p<0.001$. Two-way ANOVA with Šídák's multiple comparisons test, significance per timepoint between genotypes (A); Student's t test (B-G).

Fig.1

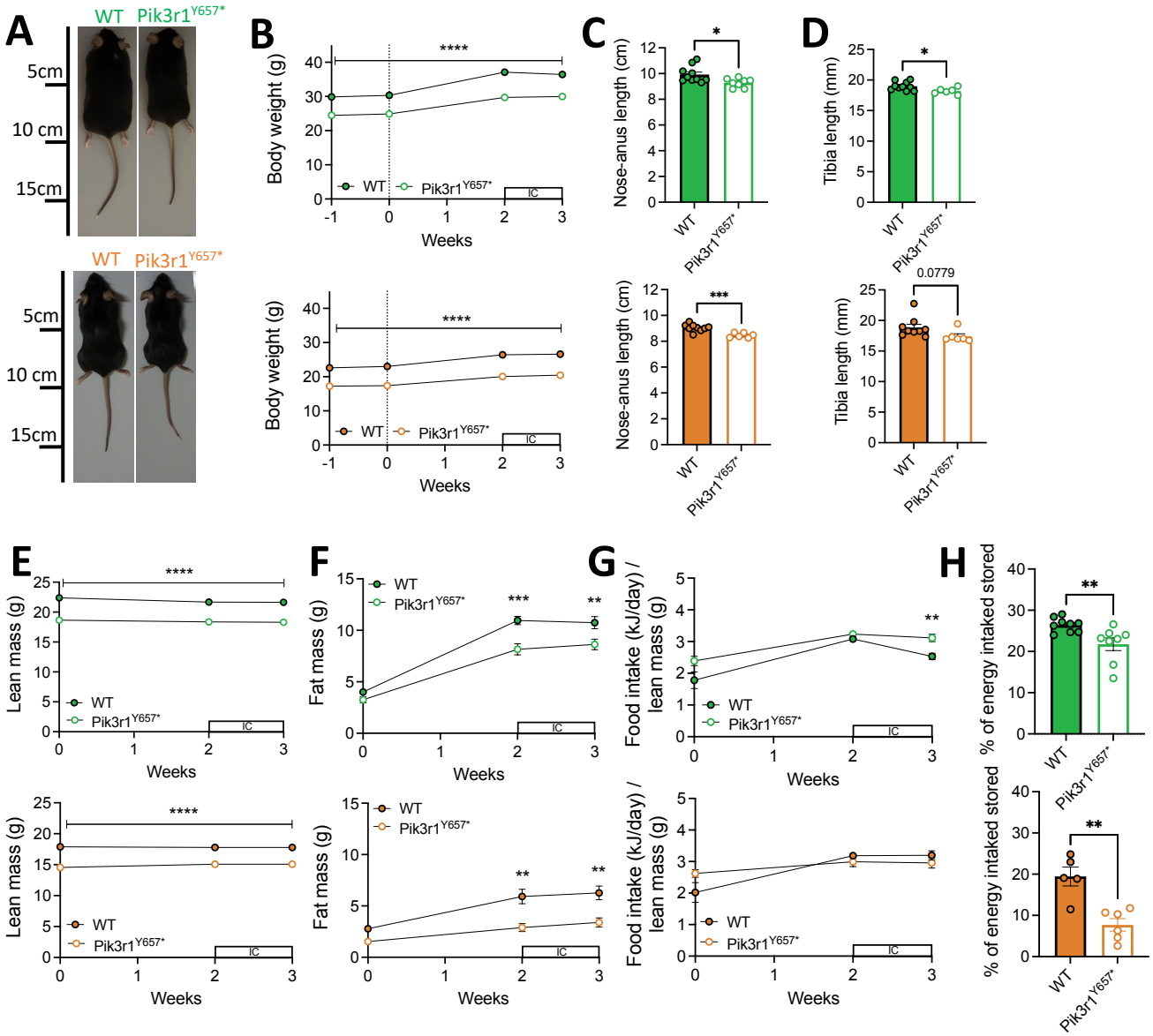
A
WT
Pik3r1Y657*
5cm
10 cm
15cm
B
Body weight (g)
Weeks
WT
Pik3r1Y657*
IC
****
C
Nose-anus length (cm)
*
***
D
Tibia length (mm)
0.0779
E
Lean mass (g)
F
Fat mass (g)
**
G
Food intake (kJ/day) / lean mass (g)
H
% of energy intaked stored

Fig. 2

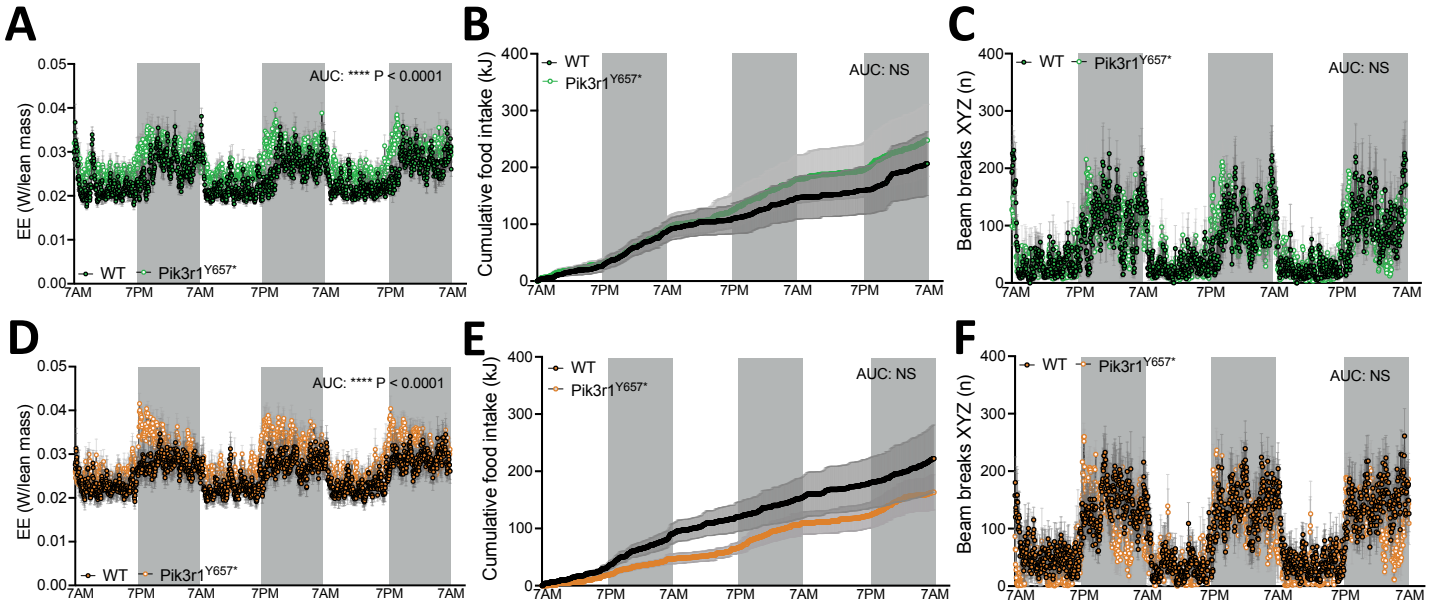
A
EE (W/lean mass)
AUC: **** P < 0.0001
WT
Pik3r1Y657*
B
Cumulative food intake (kJ)
AUC: NS
C
Beam breaks XYZ (n)
D
E
F
7AM
7PM

Fig. 3

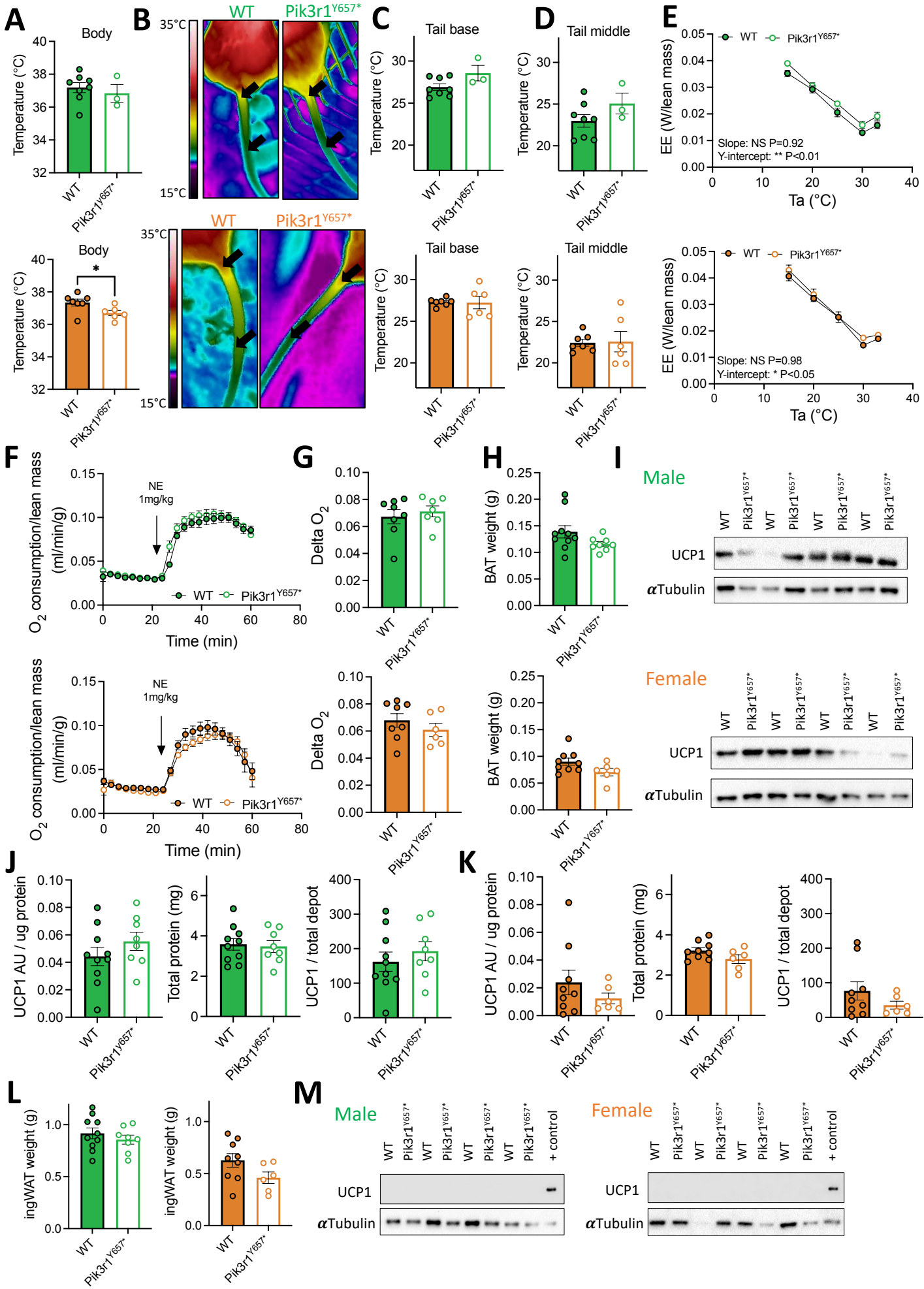
A
Body
Temperature (°C)
WT
Pik3r1Y657*
B
35°C
15°C
WT
Pik3r1Y657*
C
Tail base
D
Tail middle
E
EE (W/lean mass)
Ta (°C)
Slope: NS P=0.92
Y-intercept: ** P<0.01
Slope: NS P=0.98
Y-intercept: * P<0.05
F
NE
1mg/kg
O2 consumption/lean mass (ml/min/g)
Time (min)
G
Delta O2
H
BAT weight (g)
I
Male
Female
UCP1
αTubulin
J
UCP1 AU / ug protein
Total protein (mg)
UCP1 / total depot
K
L
ingWAT weight (g)
M
+ control

Fig. 4

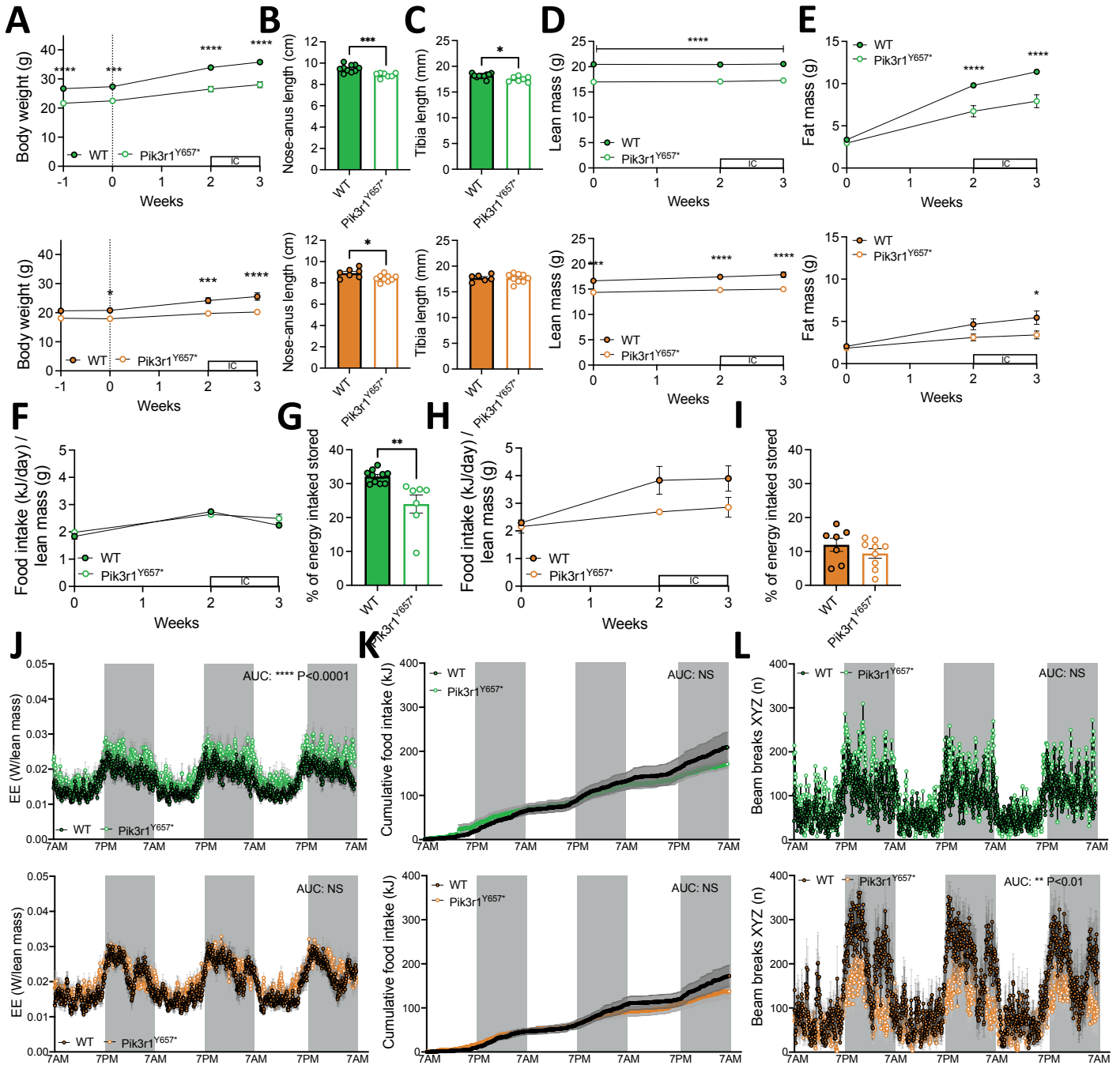
A
Body weight (g)
Weeks
WT
Pik3r1Y657*
IC
B
Nose-anus length (cm)
C
Tibia length (mm)
D
Lean mass (g)
E
Fat mass (g)
F
Food intake (kJ/day) / lean mass (g)
G
% of energy intaked stored
H
I
J
EE (W/lean mass)
AUC: **** P<0.0001
AUC: NS
AUC: ** P<0.01
K
Cumulative food intake (kJ)
L
Beam breaks XYZ (n)
7AM
7PM

Fig. 5

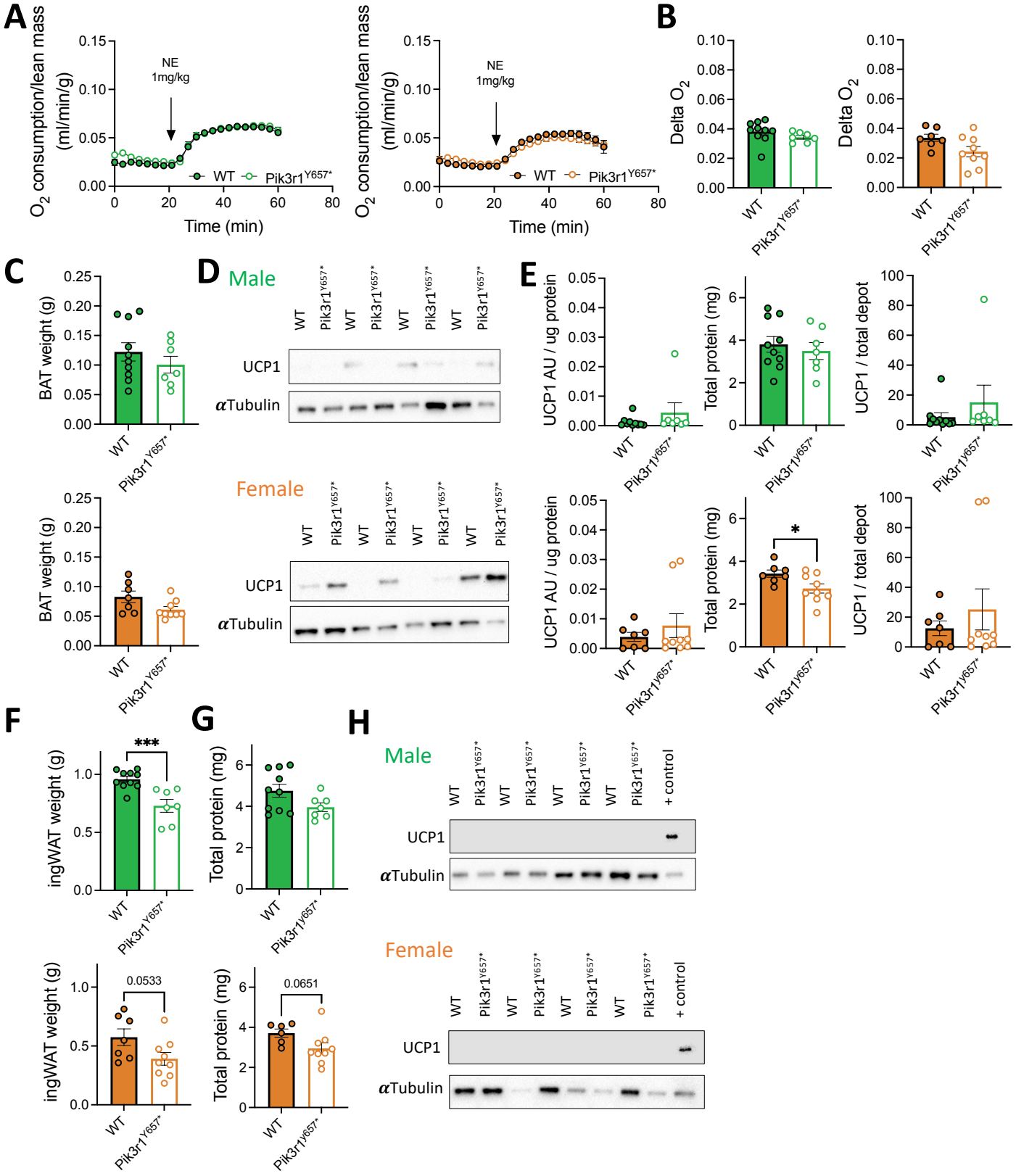
A
B
C
D
E
F
G
H
NE
1mg/kg
O2 consumption/lean mass (ml/min/g)
Time (min)
WT
Pik3r1Y657*
Delta O2
BAT weight (g)
Male
Female
UCP1
αTubulin
UCP1 AU / ug protein
Total protein (mg)
UCP1 / total depot
ingWAT weight (g)
***
0.0533
0.0651
+ control